Check for updates

Antibiofilm efficacy of a green graphene oxide-silver nanocomposite against mixed microbial species biofilms: an *in vitro* and *in silico* approach

Sadaf Aiman Khan,[abc] Amjad Almuqrin,[d] Chaminda Jayampath Seneviratne,[d] Kamal Kishore Pant, [b] [b] Zyta Maria Ziora [c] [c] and Mark A. T. Blaskovich [c] *[c]

Biofilm-related infections contribute to 65–80% of all human microbial infections, leading to significant global mortality and morbidity. In addition to their medical impact, biofilms pose serious challenges in non-medical sectors such as industrial water systems, food processing, and marine infrastructure, leading to fouling, clogging, and contamination. In this study, a biologically synthesized, non-toxic and eco-friendly reduced graphene oxide-silver nanocomposite (rGO/AgNPs) was applied to prevent microbial biofilm formation. The nanocomposite demonstrated potent antimicrobial and antibiofilm activities against single and mixed bacterial and fungal species such as Gram-positive bacteria (*Staphylococcus aureus* and *Streptococcus mutans*), Gram-negative bacteria (*Pseudomonas aeruginosa*), and a fungal species (*Candida albicans*). Crystal violet assays and scanning electron microscopy confirmed a significant reduction (50–70%) in biofilm biomass. Molecular docking studies further demonstrated robust binding of AgNPs to biofilm-associated proteins, supporting their mechanism of action. These findings demonstrate the potential of green rGO/AgNPs nanocomposites for broad-spectrum antibiofilm applications in both clinical and industrial settings, offering a sustainable strategy for future antimicrobial material development.

Sustainability spotlight

Biofilm-related microbial contamination poses significant challenges in healthcare, water treatment, and industrial systems, contributing to antimicrobial resistance and infrastructure degradation. Addressing this issue requires environmentally sustainable and effective antimicrobial strategies. This study presents a green approach to biofilm inhibition using a biologically synthesized reduced graphene oxide-silver nanocomposite (rGO/AgNPs), offering a non-toxic and eco-friendly alternative to conventional antimicrobial treatments. The research advances sustainability by utilizing waste-derived plant extracts for nanocomposite synthesis, reducing reliance on hazardous chemicals. This work aligns with the United Nations Sustainable Development Goals, particularly SDG 6 (Clean Water and Sanitation), through improved water quality and SDG 12 (Responsible Consumption and Production), by promoting green nanotechnology in biofilm prevention.

1. Introduction

Microbes spend much of their lives within biofilms, microbial communities that adhere to both living tissues and non-living surfaces. A biofilm is a structured community of microbial cells encased within a self-produced extracellular polymeric substance (EPS), primarily consisting of proteins, extracellular polysaccharides, and nucleic acids.[1] The EPS shields the bacteria from the outside environment, making it difficult to kill them with common antibiotics or chemicals.[2] Biofilm progresses through three distinct stages: (i) attachment, (ii) growth and maturation, and (iii) dispersion. Biofilms exhibit resistance to antimicrobials because (1) the antimicrobial agents face challenges in penetrating the biofilm structure, (2) the development of intricate drug resistance properties through evolution, and (3) biofilm-mediated inactivation or modification of antimicrobial enzymes.[3,4] The microorganisms within a biofilm can also exist in a reduced metabolic state, reducing their susceptibility to antibiotics acting on metabolic pathways.

Microorganisms within biofilms are more challenging to eliminate than free-floating microorganisms and lead to persistent infections.[5–7] The National Institutes of Health and the Centers for Disease Control report that biofilm-forming Gram-negative bacteria, including *Escherichia coli*, *Pseudomonas aeruginosa*, *Klebsiella pneumoniae*, and *Proteus mirabilis*,

[a]The University of Queensland - Indian Institute of Technology Delhi Academy of Research (UQIDAR), Brisbane, Australia

[b]2 Department of Chemical Engineering, Indian Institute of Technology Delhi, New Delhi 110016, India

[c]3 Centre for Superbug Solutions, Institute for Molecular Bioscience, The University of Queensland, St Lucia QLD 4072, Australia. E-mail: m.blaskovich@uq.edu.au

[d]School of Dentistry, The University of Queensland, Herston QLD 4006, Australia

along with Gram-positive bacteria such as *Staphylococcus aureus*, *Enterococcus*, and *Bacillus* spp., are responsible for 65–80% of infectious diseases.[8,9] These biofilms can be formed by both single and multiple microbial species and exhibit heightened resistance to antimicrobials compared to freely suspended planktonic cultures, making antibiofilm treatment a challenging task.[10] Notably, it is not just bacteria that can form biofilms, with fungi such as *Candida albicans* also existing in a biofilm form. Annually, 90.4 billion dollars are spent for uncontrolled biofilms in water distribution systems, which both present health hazards and reduce the efficiency of water delivery. Hence, the National Biofilm Innovation Center (UK) suggests that there is an urgent need to identify new methods to prevent biofilm formation.[11]

While many studies have focused on mono-species biofilms, it is important to note that *C. albicans* can also contribute to the formation of polymicrobial biofilms alongside other microorganisms at infection sites. Among bacteria-fungi polymicrobial biofilms, *Candida* spp. is frequently found, and various investigations have demonstrated an increased lethality associated with polymicrobial biofilms.[12,13] In polymicrobial biofilms, microorganisms can engage in mutualism, antagonism, and commensalism. Notably, *C. albicans* and *P. aeruginosa* commonly form polymicrobial biofilms, particularly in the lungs of individuals with cystic fibrosis.[14] Dental plaques and the urinary tract frequently harbour mixed biofilms of *C. albicans* and *E. coli*, exhibiting increased adhesion compared to mono-biofilms formed from the individual pathogens.[15,16] Additionally, coexistence of *C. albicans* and *S. aureus* populations has been observed under conditions such as denture stomatitis, periodontitis, and burn wound infections.[17] Moreover, *C. albicans* and *Klebsiella pneumoniae* have been found coexisting in biofilms.[18] Antimicrobial resistance in biofilms can emerge due to polymicrobial interactions and complex genetic and molecular mechanisms.[19] Since targeting a single species in polymicrobial biofilms may not lead to biofilm disruption, the efficacy of broad-spectrum antimicrobials is essential for eliminating all pathogens within these biofilms.[20]

In recent years, numerous laboratory methods have been developed to assess treatments aimed at addressing biofilm formation, indicating a growing interest in conducting antimicrobial susceptibility testing within biofilms. Various methodologies have been introduced, including estimation of minimal biofilm eradication concentration (MBEC), minimal biofilm inhibitory concentration (MBIC), biofilm bactericidal concentration (BBC), and biofilm prevention concentration (BPC).[21] MBIC, MBEC, and BBC are used to investigate the antimicrobial impact on preformed biofilms. Similar to the minimum inhibitory concentration determined for planktonic bacteria, MBIC refers to the minimum concentration of an antimicrobial agent that prevents any time-dependent increase in the average number of viable biofilm cells. Likewise, the minimal bactericidal concentration for planktonic bacteria corresponds to MBC for biofilms, indicating the lowest concentration resulting in a 99.9% reduction in CFU of bacteria within the biofilm culture. Another test commonly employed is the minimal biofilm-eradication concentration (MBEC), which signifies the lowest

concentration of an antimicrobial agent that prevents visible growth in the recovery medium used to collect biofilm cells. Finally, the biofilm prevention concentration (BPC) involves the simultaneous addition of the antimicrobial agent and inoculum. It denotes the antimicrobial concentration at which either the cell density of a planktonic culture is adequately reduced to prevent biofilm formation, or the planktonic bacteria are inhibited from converting into a biofilm state.[22]

Nanoparticles have been extensively researched for their intrinsic antibacterial properties, but investigations into their use for biofilm control are relatively new. The EPS matrix's role in the biofilm–nanoparticle interaction is of particular interest. Because of the presence of a complex EPS matrix, phenomena like nanoparticle adsorption and diffusion become extremely important.[23] Many researchers have reported that the mechanism of AgNPs' bactericidal activity is due to the release of Ag^+ ions, but only a few have investigated AgNP particle-specific activity.[24,25] According to these findings, AgNPs may have greater bactericidal activity than Ag^+ ions. As a result, the bactericidal effects of AgNPs rather than the release of Ag^+ ions for disinfection activity must be investigated.

While the antimicrobial properties of silver nanocomposites have been widely studied, their effectiveness against mixed microbial biofilms, consisting of both bacteria and fungi, has received limited attention. Moreover, our previous work demonstrated the photocatalytic potential of this green-synthesized rGO/AgNPs nanocomposite for paraben degradation. In contrast, the current study represents the first report on its broad-spectrum antibiofilm efficacy, highlighting its novel application in microbial biofilm control and extending its utility from environmental remediation to biological systems.

2. Experimental

2.1. Materials

Brain heart infusion (BHI) media (CAS 110493), acetone (CAS 67-64-1), glutaraldehyde (CAS 354400), and ethanol were obtained from Merck while phosphate buffered saline (PBS), agar powder (CAS 9002-18-0), and crystal violet dye (CAS 548-62-9) were obtained from Sigma-Aldrich. All chemical reagents were used in their original form without any further purification. Deionized water was employed for aqueous preparations and other experimental procedures.

2.2. Synthesis of the green rGO/AgNPs nanocomposite and characterization

rGO-AgNPs were prepared by a green *in situ* reduction method as described in our previous work.[26] Fresh *Citrus limetta* fruit peels were collected, cut into pieces, dried overnight in an oven, and then used to make a biological green extract. This extract served as a reducing and stabilizing agent in the green synthesis of the rGO/AgNPs nanocomposite. The phytochemicals present in the peel extract facilitated the reduction of Ag^+ ions to Ag^0 nanoparticles and helped in their stabilization on the graphene oxide sheets. The synthesized nanocomposite was analysed using various characterization techniques. Transmission

electron microscopy (Hitachi HT7700 120 kV TEM) was employed to capture images, operating at a maximum accelerating voltage of 120 kV, to assess particle distribution and size. The X-ray diffraction (XRD) spectrum was attained using an X-ray diffractometer (MiniFlex, Rigaku) with Cu–K radiation as the X-ray source to investigate the crystalline nature, phase, and size of synthesized AgNPs between 10° and 90°. SEM was performed using a field emission scanning electron microscope (FE-SEM, JSM-7800F Prime, Jeol) to capture images.

2.3. Strains and growth conditions

Microorganisms were obtained from ATCC (American Type Culture Collection) and revived from glycerol stock cultures from −80 °C in BHI broth and agar plates. *Candida albicans* (SC5314), *Streptococcus mutans* (ATCC 25175), *Staphylococcus aureus* (ATCC 43300), and *Pseudomonas aeruginosa* (ATCC 27853) were used as model organisms for this study. They were incubated overnight in a 5% CO_2 atmosphere at 37 °C for 24 h with consecutive transfers. For all the assays, the bacteria were allowed to grow to the logarithmic phase before use.

2.4. Antimicrobial activity

The susceptibility of microorganisms to GO and green nanocomposite rGO/AgNPs was assessed by determining the minimum inhibitory concentration (MIC) using a broth dilution method in a microtiter plate filled with sterile BHI broth. The MIC of an antimicrobial agent is the lowest concentration that will inhibit visible growth of bacteria following an overnight incubation.

Cultures of Gram-positive bacteria (*S. mutans* and *S. aureus*), Gram-negative bacteria (*P. aeruginosa*), and a fungus (*C. albicans*) were grown overnight in 10 mL of BHI broth at 37 °C with shaking at 180 rpm from a single colony. Diluting 50 μL in 5 mL BHI and growing to the mid-log phase, a subculture of 1×10^5 CFU mL^{-1} was prepared from the overnight culture. A 96-well microplate was filled with a two-fold dilution series of 100 μL of rGO/AgNPs in BHI solution, followed by 100 μL of the subculture suspension. (The rGO/AgNP concentrations tested were 0.5, 0.25, 0.125, 0.0625, and 0.0313 mg mL^{-1}). The same procedure

was used to test GO. Positive controls containing no rGO/AgNPs and negative controls containing no bacteria or rGO/AgNPs were also included. The plates were then incubated for 20 hours at 37 °C in an incubator without shaking before visually observing the wells with growth/no growth. All experiments were carried out in triplicate.

2.5. Antibiofilm activity

The assay was carried out in 96-well microtiter plates containing microorganisms (*C. albicans*, *S. mutans*, *S. aureus*, and *P. aeruginosa*) grown simultaneously with the rGO/AgNPs nanocomposite to assess its ability to prevent formation of biofilms. The nanocomposite was suspended in BHI media with 1% sucrose and added as a two-fold dilution in the microtiter plate. Concentrations of rGO/AgNPs tested were 1, 0.5, 0.25, 0.125, 0.0625 and 0.03125 mg mL^{-1}. The overnight grown cultures of microbes were diluted and grown to the mid log phase and then diluted to 1×10^7 CFU mL^{-1} 100 μL of aliquot of culture was added to each well containing 100 μL of nanocomposite rGO/AgNPs. The plates were incubated for 24 h with shaking at 37 °C. GO was tested in the same manner. Positive controls containing no rGO/AgNPs and negative controls containing no bacteria or rGO/AgNPs were also included.

For the mixed species antibiofilm analysis, a mixture of fungal and bacterial culture was added to the well in a 1 : 1 ratio to make a final culture aliquot of 100 μL. After incubation, the plates were subjected to crystal violet (CV) assay for analysis. The CV assay estimated the BPC (biofilm prevention concentration) of rGO/AgNPs against each bacterium in the exponential phase. The BPC is defined as the lowest antimicrobial concentration that results in a significant reduction in biofilm formation. All experiments were carried out in triplicate. Fig. 1 presents a schematic representation of the protocol for the antibiofilm formation activity assay for the rGO/AgNPs nanocomposite.

2.6. Crystal violet assay

Following the incubation period, the plates were tested to analyze the antibiofilm effects using the CV assay. The
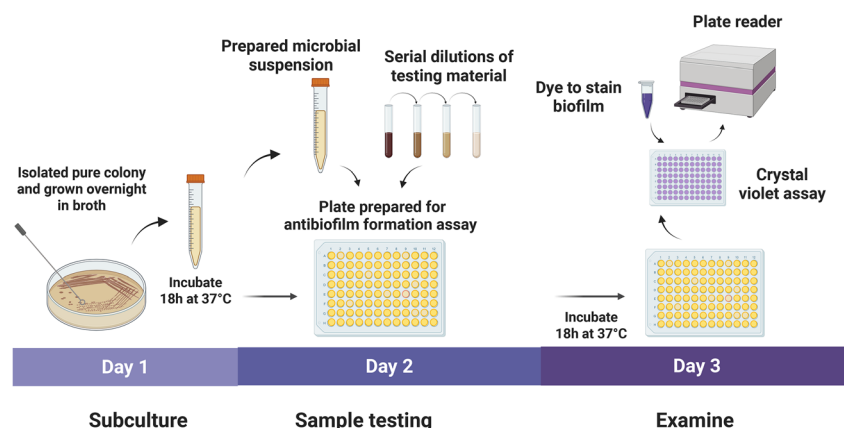

Fig. 1 Schematic representation of the protocol for the antibiofilm formation activity assay for rGO/AgNPs nanocomposite.

suspensions were carefully removed from the 96 well plate and rinsed with PBS to remove any planktonic bacteria. Following that, a 1% (w v^{-1}) CV dye solution was added to each well and incubated for 30 minutes to quantify the remaining biofilm. The dye was removed, and any remaining dye was washed away with PBS. The stained biofilms were dissolved in 10% (v/v) acetic acid, and the absorbance of the yielding solution at 590 nm was measured using a microplate reader (TECAN Infinite 200 Pro).

The percentage of biofilm biomass reduction was measured using the equation:

$$\text{Biofilm biomass reduction}\% = [(\text{control OD}_{570nm} - \text{test OD}_{570nm})/\text{control OD}_{570nm}] \times 100$$

2.7. Scanning electron microscopy

For SEM analysis, the cultures were grown on coverslips placed in a 12 well plate along with the most effective concentration of the rGO/AgNPs suspension as observed in the CV assay. After incubation, the samples were rinsed with $1 \times$ PBS and fixed with 2.5% glutaraldehyde for 15 min in an ascending series of 50%, 70%, 85%, 90%, and 100% ethanol. The samples were dehydrated, air-dried, and carefully mounted on a stub with carbon tape. Samples were introduced into a sputter coater chamber and coated with a very thin layer of platinum and then examined with a scanning electron microscope (Hitachi HT7700 120 kV TEMs) with a voltage of 120 kV as maximum accelerating voltage. Control samples with no nanomaterial addition were also prepared for comparison.

2.8. Molecular docking

An *in silico* approach using molecular docking studies was employed to investigate the potential molecular interactions between AgNPs and proteins involved in biofilm formation in *S. aureus* SdrC and SasG, in *S. mutans* GtfB and SrtA, in *P. aeruginosa* LasR and PelB, and in *C. albicans* Asl3 and CYP51. The protein crystal structures were obtained from the Protein Data Bank (PDB) database (**https://www.rcsb.org**), while the 3D structure of AgNPs was retrieved from a previous study.[27] The AgNPs were constructed using molecular dynamics simulation using Gromacs 2019v with energy minimisation. The PDB file of AgNPs is included in the SI.

In the present study, the interactions of the target ligand (AgNPs) with microbial proteins involved in biofilm formation were analysed using Hex 8.0.0 docking software.[28] Hex is a molecular graphics program that calculates and displays possible docking modes for pairs of proteins, DNA molecules, and other ligand compounds. It can also compute protein–protein docking, protein–ligand docking (assuming that the ligand is rigid), and superpose pairs of molecules using only their 3D shapes. The software used a fast Fourier transformation algorithm to provide the protein receptor's closest binding energy conformations with the ligand *via* electrostatic protein interactions and steric shape. The grid was constructed from stabilized conformational space. Post-docking analyses for conformational clustering were performed and visualized using
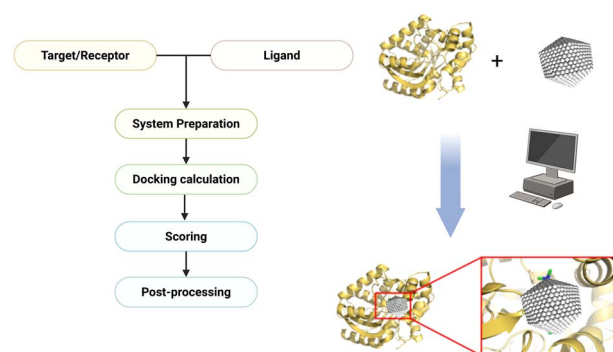

Fig. 2 The series of steps for a particular docking process.

the UCSF Chimera and PyMol software. The various steps involved in docking are presented in Fig. 2.

Docking predictions were optimized by adjusting multiple parameters, including correlation type (shape + electrostatics), FFT mode (3D), grid dimension (0.6), receptor range (180), ligand range (180), twist range (360), and distance range (40). Binding energy values (in kJ mol^{-1}) were then calculated.

2.9. Statistical analysis

Statistical analyses were conducted utilizing GraphPad Prism 9 (GraphPad Software, La Jolla, CA, United States), employing a two-way ANOVA followed by Tukey's multiple comparisons test to compare treatments with the control and among different treatments. The results were expressed as mean $\pm$ standard deviation. Significance levels were determined using Tukey's multiple range tests, with P values < 0.05 denoted as significant (*) and P values < 0.01 as highly significant (***).

3. Results and discussion

3.1. Synthesis of the rGO/AgNPs nanocomposite and its characterization

A reduced graphene oxide-silver nanoparticles (rGO/AgNPs) nanocomposite was produced through the simultaneous reduction and stabilization of silver nanoparticles on the surface of graphene oxide, facilitated by *Citrus limetta* peel extract. The graphene oxide nanosheets function as a substrate for the reduction of silver, leading to the formation of silver nanoparticles through the transfer of electrons by the reducing agent present in the extract. In our previous investigation,[26] the synthesized nanocomposite was applied for photocatalytic purposes and subjected to characterization to identify suitable characteristics for degradation. In the present study, the nanocomposite was further characterized to verify the presence and distribution of AgNPs on the layer of reduced graphene oxide, specifically for its application in antibiofilm activity.

The rGO/AgNPs nanocomposite was subjected to characterization through TEM, XRD, and nanoparticle size distribution analysis using ImageJ software. The morphological features of both GO and rGO/AgNPs were examined through TEM. The TEM micrograph of GO (Fig. 3(a)) revealed a singular layer of
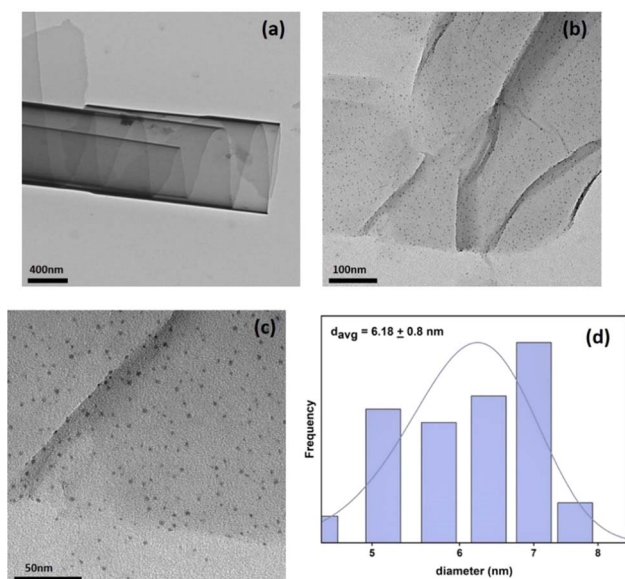
Fig. 3 TEM micrographs of (a) GO and (b and c) rGO/AgNPs with low and high magnification; (d) particle size distribution of AgNPs on the surface of rGO.
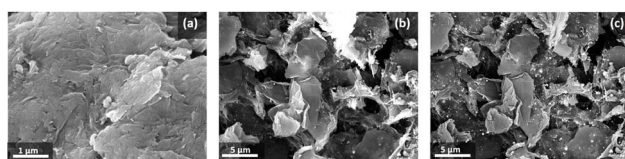

Fig. 4 (a) FESEM images of GO and rGO/AgNPs at (b) low magnification and (c) high magnification indicating the presence of AgNPs on the surface of rGO.

graphene oxide sheet. In contrast, the images of rGO/AgNPs (Fig. 3(b and c)) showcased well-dispersed silver nanoparticles embellishing the surface of GO nanosheets. The average size of the AgNPs was approximately 6 nm (Fig. 3(d)). These results affirm that graphene oxide acts as a supportive agent for silver nanoparticles, simultaneously preventing their agglomeration, a drawback in conventional AgNP synthesis.[29] SEM analysis further elucidated the morphological characteristics of GO (Fig. 4(a)) and the rGO/AgNPs nanocomposite (Fig. 4(b and c)), confirming the uniform distribution of AgNPs over the surface of reduced graphene oxide layers.

Furthermore, XRD analysis confirmed the crystal structure of AgNPs. The graph depicted in Fig. 5 displays four distinctive peaks for AgNPs that are not present in the GO sheets. The four distinct peaks specific to the rGO/AgNPs nanocomposite, observed at $2\theta^\circ$, were at 38.10, 44.28, 64.48, and 77.34, corresponding to the (111), (200), (220), and (311) lattice planes. These peaks signify the face-centered cubic (fcc) structure planes of AgNPs (JCPDS no. 04-0783), indicating the successful formation of metallic silver nanoparticles.[30]

Unlike earlier reports that focused on photocatalytic or antibacterial effects of similar nanomaterials, the present study explores the unique application of this green rGO/AgNPs
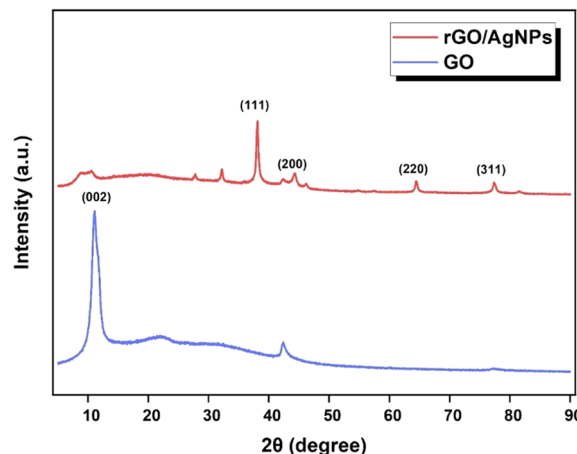

Fig. 5 XRD patterns of GO and the rGO/AgNPs nanocomposite showing distinct peaks of metallic Ag in the composite.

nanocomposite in disrupting complex microbial biofilms, including dual-species models, which was not previously demonstrated.

3.2. MIC determination by broth microdilution assay

The antimicrobial efficacy of the green rGO/AgNPs nanocomposites was evaluated against *S. aureus*, *S. mutans*, *C. albicans*, and *P. aeruginosa*. Various concentrations of rGO/AgNPs nanocomposites were incubated overnight with each microbial species in 96-well plates, and the inhibitory concentrations were assessed based on bacterial absorption. A negative control was included, consisting of the medium without the nanocomposite. The rGO/AgNPs nanocomposites exhibited effectiveness against Gram-positive *S. mutans* (0.03125 mg mL^{-1}), *S. aureus* (0.0625 mg mL^{-1}), and Gram-negative *P. aeruginosa* (0.0625 mg mL^{-1}). Despite differences in their biological structures, the antimicrobial effects against these bacteria showed minimal variation. Gram-positive bacteria feature a thick cell wall primarily composed of peptidoglycans, while Gram-negative bacteria have an outer membrane consisting of lipopolysaccharides, lipoproteins, and complex polymers, along
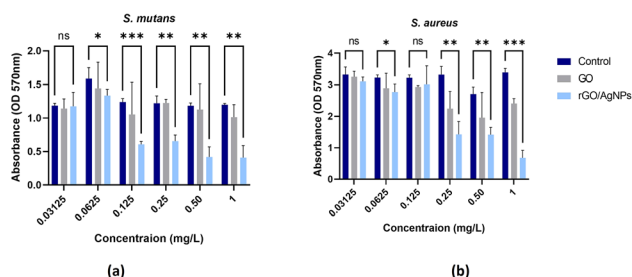

Fig. 6 Antibiofilm effects of rGO/AgNPs on mono-species biofilms of *S. mutans* (a) and *S. aureus* (b), at concentrations of 0.03125, 0.0625, 0.125, 0.25, 0.5, and 1 mg mL^{-1}, obtained by CV assay. ($n = 3$, data are mean + SD and representative of three or four independent experiments; multiple *t* tests; ns, not significant; *$P < 0.05$; **$P < 0.01$; ***$P < 0.001$).

with a thinner peptidoglycan layer. Due to the limited penetration of antimicrobial agents through their outer membrane, Gram-negative bacteria generally demonstrate greater resistance compared to Gram-positive bacteria. The antifungal efficacy of the green rGO/AgNPs nanocomposite was assessed against *C. albicans*, demonstrating antifungal activity at a concentration of 0.0625 mg mL^{-1}, consistent with the level of antibacterial activity. The stabilization of AgNPs on GO sheets creates an improved platform for nanoparticle–microbe interactions.[31] Research has shown that the antibacterial activity of graphene nanocomposites is primarily attributed to the nonspecific binding ability of GO sheets to microbial cells.[32]

3.3. Antibiofilm activity of the green nanocomposite

The antibiofilm formation abilities of the rGO/AgNPs were assessed against bacterial and fungal strains. Notably, the presence of rGO/AgNPs significantly reduced the biofilm-forming ability of both strains. A biofilm assay was conducted to evaluate the effectiveness of these composite compounds in inhibiting biofilm formation.

The antibiofilm potential was explored across various microbial species at different concentrations (0.03125, 0.0625, 0.125, 0.25, 0.5, and 1 mg mL^{-1}) added simultaneously with inoculum. Following 24 hours of incubation, bacterial cultures treated with either GO or rGO/AgNPs exhibited restrained biofilm formation in contrast to the control group. Notably, the nanocomposite rGO/AgNPs demonstrated superior efficacy compared to GO alone. Biofilm reduction was directly quantified from the microtiter plate using the crystal violet complex. The shaking of the microtiter plate during the incubation period is also an important factor for biofilm growth. It improves oxygen and nutrient diffusion and promotes heterogeneity which boosts the cellular growth as well as EPS production. It has been reported that under shaking conditions the biofilms grow 2 logs higher as compared to static conditions.[33,34] This makes the antibiofilm effect different from simple antimicrobial effects which are tested at low concentrations of microbial counts under static conditions.

The dose-dependent antibiofilm formation effects of GO and rGO/AgNPs were examined towards single species biofilms of

Gram-positive bacteria *S. aureus* and *S. mutans* under *in vitro* conditions (Fig. 6). For *S. mutans*, rGO/AgNPs showed significant reduction in biofilm biomass (about 50.9%) in comparison to the control at a concentration of 0.125 mg mL^{-1}. Similarly,
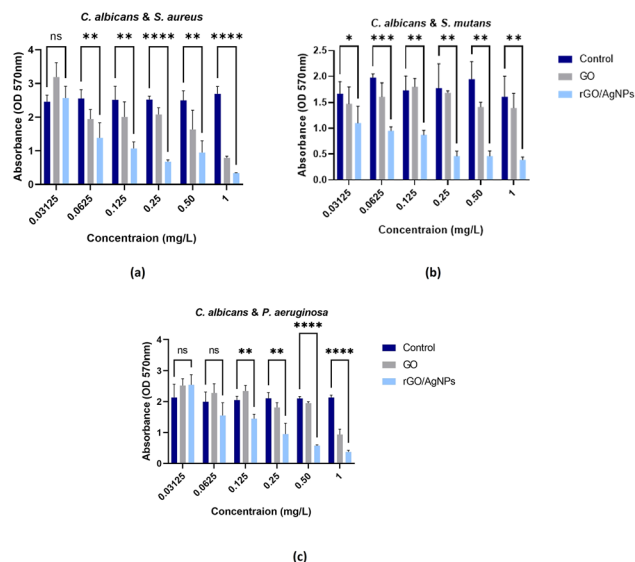

Fig. 8 Antibiofilm effects of rGO/AgNPs on mixed species biofilms of *C. albicans*-*S. aureus* (a), *C. albicans*-*S. mutans* (b) and *C. albicans*-*P. aeruginosa* (c), at concentrations of 0.03125, 0.0625, 0.125, 0.25, 0.5, and 1 mg mL^{-1}, obtained by CV assay. ($n = 3$, data are mean + SD and representative of three or four independent experiments; multiple t tests; ns, not significant; *$P < 0.05$; **$P < 0.01$; ***$P < 0.001$; ****$P < 0.0001$).
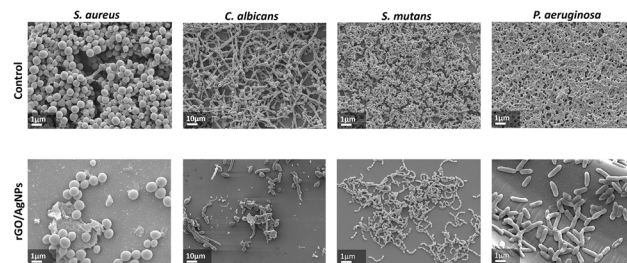

Fig. 9 SEM micrographs of the control and rGO/AgNPs treated biofilms of single microbial species.

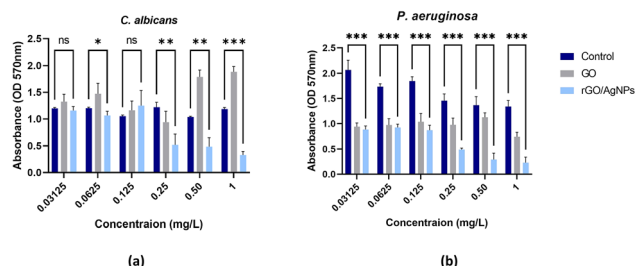Fig. 10 SEM micrographs of the control and rGO/AgNPs treated biofilms of mixed microbial species biofilms.

Fig. 7 Antibiofilm effects of rGO/AgNPs on mono-species biofilms of *C. albicans* (a) and *S. aureus* (b), at concentrations of 0.03125, 0.0625, 0.125, 0.25, 0.5, and 1 mg mL^{-1}, obtained by CV assay. ($n = 3$, data are mean + SD and representative of three or four independent experiments; multiple t tests; ns, not significant; *$P < 0.05$; **$P < 0.01$; ***$P < 0.001$).
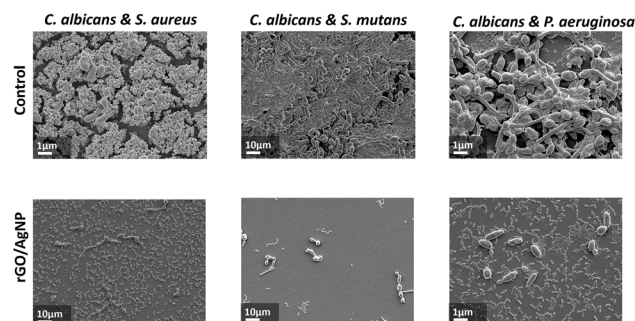
for *S. aureus*, a significant reduction in biofilm biomass (about 56.9%) was observed at a 0.25 mg mL^{-1} concentration of rGO/AgNPs.
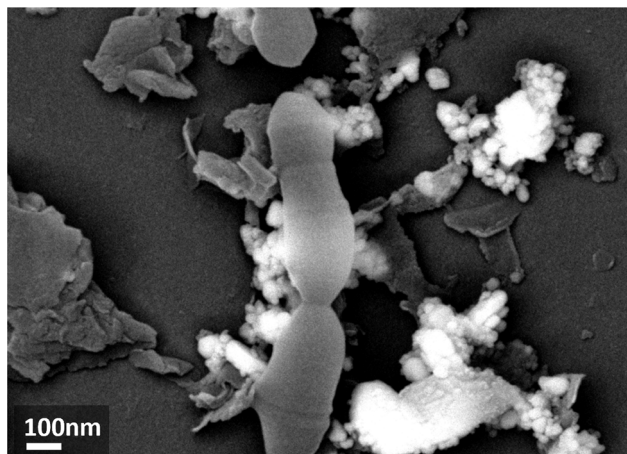

Fig. 11 Magnified view of interaction of AgNPs of the nanocomposite with the bacterial cell (*S. mutans*).
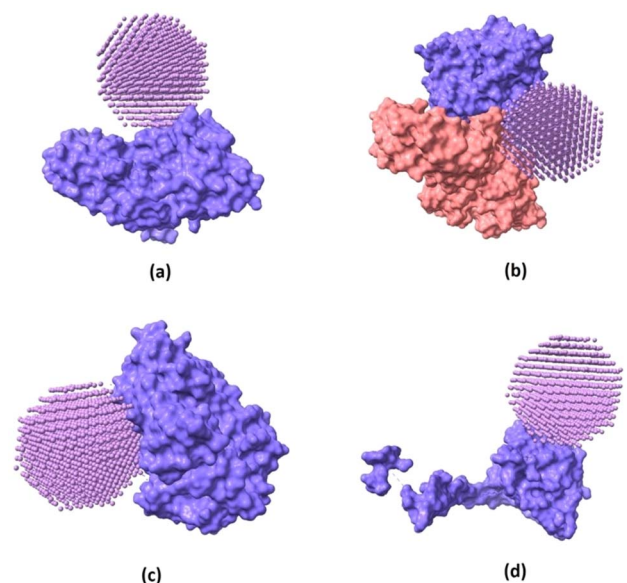

Fig. 12 Molecular docking analysis of AgNPs with biofilm associated proteins of *S. aureus* (a) SdrC, (b) Bap and S. mutans, (c) GtfB and (d) SrtA.

C. albicans was evaluated as the fungal single species, with nanocomposite treatment leading to significant reduction in biofilm biomass (57%) at a concentration of 0.25 mg mL^{-1} (Fig. 7). *P. aeruginosa*, as a model Gram negative bacterium, showed a significant reduction in single species biofilm biomass (66%) at the same concentration (Fig. 7). These data indicate that AgNPs impede biofilm formation of bacteria and fungi. These findings are consistent with the observations of Namasivayam and Roy,[35] who reported that chemogenic silver nanoparticles stabilized with chitosan exhibited enhanced antibiofilm activity against *E. coli*. Similarly, Jena *et al.*[36] suggested that the increased antibiofilm efficacy of chitosan-stabilized metallic nanoparticles could be due to the inhibition of exopolysaccharide synthesis, which restricts biofilm formation, or the diffusion of AgNPs through biofilm channels, enabling the sustained release of metal nanoparticles and their subsequent antimicrobial effects.

Biofilms in real environments are not single species but a mixture of species. To replicate that, the biofilms formed from a mixture of bacterial and fungal species were tested to evaluate the antibiofilm efficacy of the green rGO/AgNPs nanocomposite. Concentrations of 0.25 mg mL^{-1} showed significant reduction (77%) in both mixed species biofilms of *C. albicans* – *S. aureus* and *C. albicans* – *S. mutans*, while 0.5 mg mL^{-1} of rGO/AgNPs was required for 62% reduction in biofilm biomass of the mixed species of *C. albicans*-*P. aeruginosa* (Fig. 8). This increased concentration needed for biofilms containing the Gram-negative pathogen could be attributed to the nature of the bacterial cell wall, but potentially also to the synergy between the different species in the biofilm.

Notably, GO individually did not exhibit any significant antibiofilm activity against *S. aureus*, *S. mutans* or *C. albicans*, and the inhibition seen against *P. aeruginosa* did not vary with concentration, suggesting that the major antibiofilm effects observed resulted from the AgNPs. Previous research has also documented the inhibition of biofilm formation by AgNPs. For example, AgNPs synthesized from *Momordica charantia* extract demonstrated enhanced anti-biofilm activity against *E. faecalis* and *A. hydrophilia*. Furthermore, the antibiofilm activity of AgNPs was linked to their diffusion through biofilms, leading to antimicrobial effects.[37]

AgNPs are also known for their ability to inhibit the synthesis of the glycocalyx matrix, a key component of bacterial biofilms, and for disrupting quorum sensing molecules, which play a vital role in the signalling system that promotes biofilm formation.[38–40]

Table 1 Biofilm associated proteins from various species and their docking with AgNPs

Microbial species	Protein	Role in biofilms	RCBS ID	E value (KJ mol^{-1})
S. aureus	SdrC	Host tissue colonization and virulence	6LXS	−434.35
	Bap	Involved in adherence	7C7U	−334.50
S. mutans	GtfB	Colonization and EPS matrix formation	8FKL	−482.08
	SrtA	Cell adhesion	4TQX	−391.33
C. albicans	Asl3	Cell adhesion for biofilm formation	4LEE	−396.73
	CYP51	Cell membrane structure	5V5Z	−551.07
P. aeruginosa	LasR	Quorum sensing	2UV0	−493.04
	PelB	Cell–cell interaction in the biofilm matrix	5WFT	−425.97

Although our study focuses on evaluating the efficacy of green-synthesized rGO/AgNPs nanocomposites, we also reviewed relevant literature to place our findings in context with conventional antibiofilm agents. Chlorhexidine, a widely used disinfectant, typically reduces biofilm biomass by 40–60% in similar *in vitro* models, while silver nitrate solutions often show species-specific efficacy but lack the broad-spectrum performance observed here. In comparison, our rGO/AgNPs nanocomposite achieved 50–70% biofilm reduction at 0.25 mg mL^{-1}, including against mixed-species biofilms, highlighting its potential as a more sustainable and versatile alternative. Future studies will include direct comparisons with such conventional agents under identical experimental conditions.[41–43]

3.4. SEM analysis

SEM micrographs of the single and mixed species biofilms of control and nanocomposite treatment were analysed. As shown in Fig. 9, the results show an apparent decrease in biofilm architecture after treatment with rGO/AgNPs in cases of single *S. aureus*, *S. mutans*, *C. albicans* and *P. aeruginosa* biofilms compared to untreated control biofilms. Biomass reduction was also observed for the mixed species biofilms of *C. albicans* – *S. aureus*, *C. albicans* – *S. mutans* and *C. albicans-P. aeruginosa* for the nanocomposite treated biofilms as compared to untreated biofilms, as presented in Fig. 10.

The treated cell surface had more roughness and there was minimal EPS matrix present. The SEM also showed reduced cell adhesion and microbial colonization. A magnified view of bacterial cells (*S. mutans*) is also presented in Fig. 11 that shows the interaction of cells with AgNPs in the dark field microscopic view. The fungal species *C. albicans* showed remarkable morphological changes as the control had more hyphal forms in comparison to nanocomposite treated biofilms.
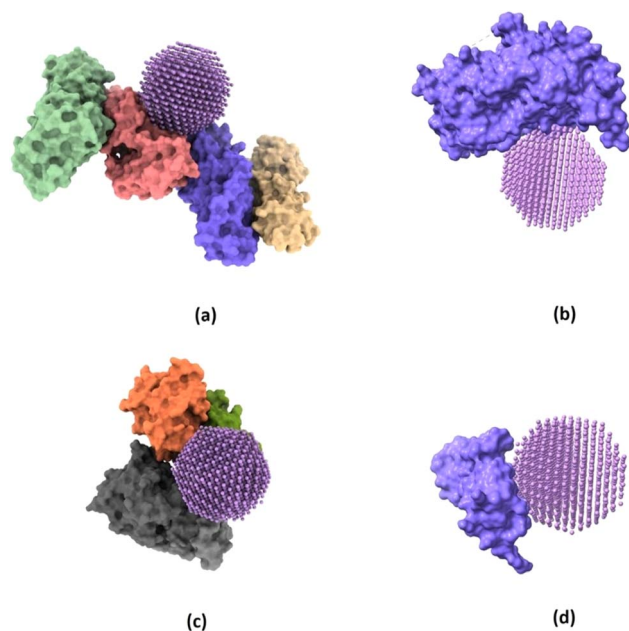

Fig. 13 Molecular docking analysis of AgNPs with biofilm associated proteins of *C. albicans*, (a) Asl3, (b) CYP51 and *P. aeruginosa*, (c) LasR and (d) PelB.
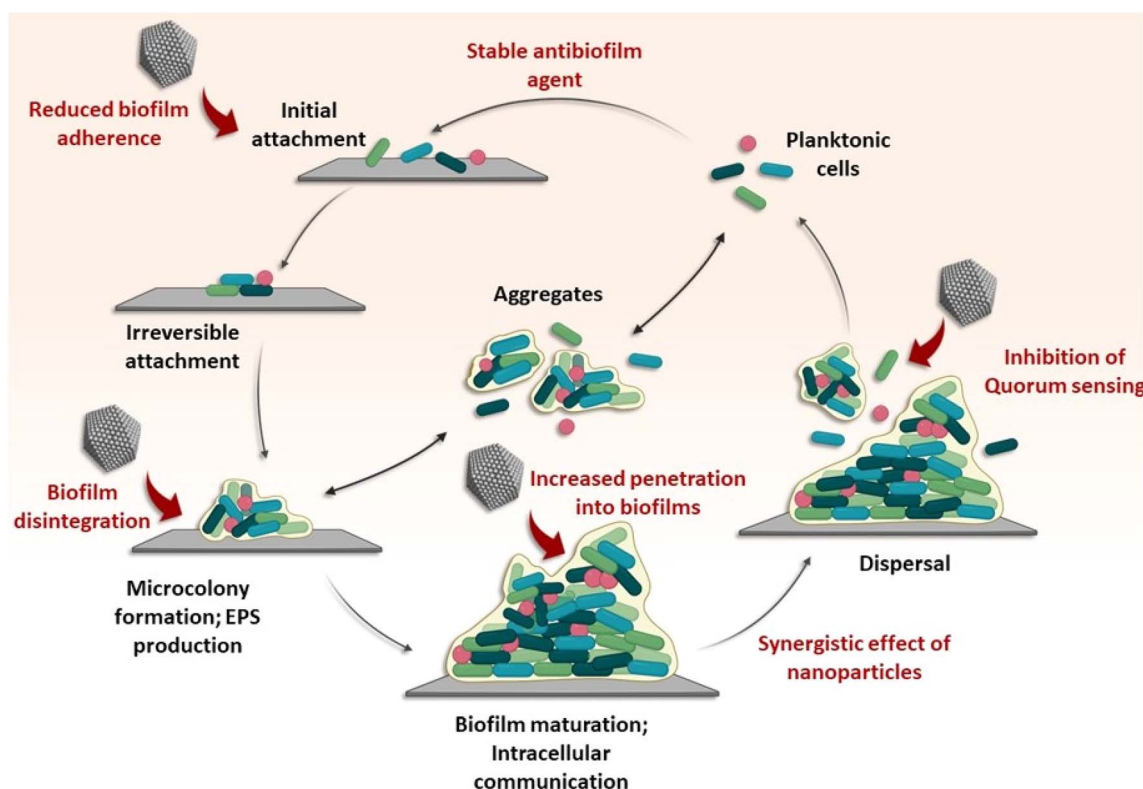

Fig. 14 Schematic representation of the various mechanisms involved in the action of AgNPs for the antibiofilm efficacy.

3.5. Molecular docking analysis

To understand the potential mechanism of antibiofilm action and predict plausible molecular-level biological interactions between AgNPs and various biofilm-associated proteins of *S. aureus*, *S. mutans*, *C. albicans* and *P. aeruginosa*, an *in silico* molecular docking study was undertaken.

These molecular docking studies aimed to provide insights into the inhibitory action of AgNPs on the key enzymes involved in biofilm formation. Unlike Ag^+ ions or Ag metal, which are commonly studied by researchers, AgNPs were employed as ligands for the *in silico* docking studies. The Hex docking software was employed to examine the interactions between the target protein and ligand. A total of 3000 solutions were modeled, and the software presented the solutions with the highest binding energies. A more negative *E* total value indicates a robust interaction between the AgNPs and target protein, resulting in the inhibition of receptor activity.[44]

The docked structures of AgNPs with the biofilm associated proteins are presented in Fig. 12 for *S. aureus* and *S. mutans* and in Fig. 13 for *C. albicans* and *P. aeruginosa*. Table 1 presents the proteins along with their respective *E* value scores from the docking results. The results showed strong binding of AgNPs with biofilm associated proteins. The efficient binding of AgNPs to biofilm-associated proteins illustrates a potential molecular level functionality underlying the anti-biofilm activity. Based on *in silico* findings and previous literature, possible mechanisms of how AgNPs interrupt the biofilm cycle are presented in Fig. 14. These include reduced biofilm adherence, increased penetration into biofilms and disintegration of biofilms.

4. Conclusion

The rGO/AgNPs were prepared using an *in situ* reduction method based on waste *Citrus limetta* fruit peel extract in an eco-friendly, rapid, and cost-effective manner. The synthesized nanocomposite was characterised using various techniques, revealing a uniform distribution of small-sized ($\sim$6 nm) AgNPs over the surface of reduced graphene oxide. The nanocomposite exhibited antimicrobial activity against Gram-positive and Gram-negative bacteria, as well as fungal species. The anti-biofilm formation results demonstrated the superior efficacy of green rGO/AgNPs against both single- and mixed-species biofilms compared to GO alone. Notably, a concentration of 0.25 mg mL^{-1} of rGO/AgNPs displayed potent antibiofilm formation activity, leading to a significant reduction in biofilm biomass (50–70%). These results were supported by scanning electron imaging analysis, which showed clear differences between treated and untreated biofilms. Molecular docking studies revealed strong binding of AgNPs with diverse biofilm-associated proteins of *S. aureus*, *S. mutans*, *C. albicans*, and *P. aeruginosa*. This study highlights the promising potential of the green nanocomposite aimed at preventing biofilm formation due to its biocompatibility, broad-spectrum activity, and mechanism-based action. However, the study was limited to *in vitro* assessments and did not evaluate long-term stability or cytotoxicity on real-world surfaces. Future studies should investigate the application of rGO/AgNP coatings on medical devices, water filtration membranes, and industrial surfaces under realistic environmental conditions. These findings support the potential use of green rGO/AgNPs nanocomposites in both healthcare and industrial settings to address the persistent challenge of biofilm-associated contamination and fouling.

Author contributions

Sadaf Aiman Khan: conceptualization, methodology, experimental design, software, investigation, and original draft writing; Amjad Almuqrin: methodology, experimentation; Chaminda Jayampath Seneviratne: conceptualization, supervision, and review; Kamal Kishore Pant: supervision, review, and editing; Zyta Maria Ziora: manuscript review, editing, and supervision; Mark A.T. Blaskovich: manuscript review, revision, and supervision. All authors approved the publication of this version of the manuscript.

Conflicts of interest

There are no conflicts to declare.

Data availability

All the data supporting this article have been included in the manuscript or the SI.

Supplementary information is available. See DOI: **https://doi.org/10.1039/d5su00093a**.

References

1 K. Lewis, Riddle of biofilm resistance, *Antimicrob. Agents Chemother.*, 2001, **45**, 999–1007.

2 J. Jang, *et al.*, Development of Antibiofilm Nanocomposites: Ag/Cu Bimetallic Nanoparticles Synthesized on the Surface of Graphene Oxide Nanosheets, *ACS Appl. Mater. Interfaces*, 2020, **12**, 35826–35834.

3 A. Elbourne, *et al.*, The use of nanomaterials for the mitigation of pathogenic biofilm formation, *Methods Microbiol.*, 2019, **46**, 61–92.

4 Y. K. Mohanta, *et al.*, Anti-biofilm and Antibacterial Activities of Silver Nanoparticles Synthesized by the Reducing Activity of Phytoconstituents Present in the Indian Medicinal Plants, *Front. Microbiol.*, 2020, **11**, 499780.

5 N. Høiby, T. Bjarnsholt, M. Givskov, S. Molin and O. Ciofu, Antibiotic resistance of bacterial biofilms, *Int. J. Antimicrob. Agents*, 2010, **35**, 322–332.

6 S. Oliver, H. Wagh, Y. Liang, S. Yang and C. Boyer, Enhancing the antimicrobial and antibiofilm effectiveness of silver nanoparticles prepared by green synthesis, *J. Mater. Chem. B*, 2018, **6**, 4124–4138.

7 S. Gurunathan, J. W. Han, D. N. Kwon and J. H. Kim, Enhanced antibacterial and anti-biofilm activities of silver nanoparticles against Gram-negative and Gram-positive bacteria, *Nanoscale Res. Lett.*, 2014, **9**, 1–17.

8 S. F. Shi, *et al.*, Reduced Staphylococcus aureus biofilm formation in the presence of chitosan-coated iron oxide nanoparticles, *Int. J. Nanomed.*, 2016, **11**, 6499–6506.

9 N. Yadav, *et al.*, Graphene Oxide-Coated Surface: Inhibition of Bacterial Biofilm Formation due to Specific Surface-Interface Interactions, *ACS Omega*, 2017, **2**, 3070–3082.

10 S. M. Santhosh and K. Natarajan, Antibiofilm Activity of Epoxy/Ag-TiO2 Polymer Nanocomposite Coatings against Staphylococcus Aureus and Escherichia Coli, *Coatings*, 2015, **5**, 95–114.

11 National Biofilm Innovation Center, *The National Biofilms Innovation Centre Annual Report*, 2022, DOI: 10.5258/biofilms/008.

12 C. J. Nobile and A. D. Johnson, Candida albicans Biofilms and Human Disease, *Annu. Rev. Microbiol.*, 2015, **69**, 71–92.

13 R. Rajendran, *et al.*, Biofilm formation is a risk factor for mortality in patients with Candida albicans bloodstream infection—Scotland, 2012–2013, *Clin. Microbiol. Infection*, 2016, **22**, 87–93.

14 M. M. Harriott and M. C. Noverr, Importance of Candida-bacterial polymicrobial biofilms in disease, *Trends Microbiol.*, 2011, **19**, 557–563.

15 M. A. El-Azizi, S. E. Starks and N. Khardori, Interactions of Candida albicans with other Candida spp. and bacteria in the biofilms, *J Appl. Microbiol.*, 2004, **96**, 1067–1073.

16 M. Hacioglu, O. Oyardi, C. Bozkurt-Guzel and P. B. Savage, Antibiofilm activities of ceragenins and antimicrobial peptides against fungal-bacterial mono and multispecies biofilms, *J. Antibiotics, - Ser. B*, 2020, **73**(7), 455–462.

17 E. Hernandez-Cuellar, *et al.*, Characterization of Candida albicans and Staphylococcus aureus polymicrobial biofilm on different surfaces, *Rev. Iberoam. Micol.*, 2022, **39**, 36–43.

18 M. L. Falsetta, *et al.*, Symbiotic relationship between Streptococcus mutans and Candida albicans synergizes virulence of plaque biofilms in vivo, *Infect. Immun.*, 2014, **82**, 1968–1981.

19 H. Koo, R. N. Allan, R. P. Howlin, P. Stoodley and L. Hall-Stoodley, Targeting microbial biofilms: current and prospective therapeutic strategies, *Nat. Rev. Microbiol.*, 2017, **15**(12), 740–755.

20 S. P. Lopes, N. F. Azevedo and M. O. Pereira, Microbiome in cystic fibrosis: Shaping polymicrobial interactions for advances in antibiotic therapy, *Crit. Rev. Microbiol.*, 2015, **41**, 353–365.

21 M. D. Macià, E. Rojo-Molinero and A. Oliver, Antimicrobial susceptibility testing in biofilm-growing bacteria, *Clin. Microbiol. Infection*, 2014, **20**, 981–990.

22 L. Thieme, *et al.*, MBEC Versus MBIC: The Lack of Differentiation between Biofilm Reducing and Inhibitory Effects as a Current Problem in Biofilm Methodology, *Biol. Proced. Online*, 2019, **21**, 1–5.

23 C. H. N. Barros and E. Casey, A Review of Nanomaterials and Technologies for Enhancing the Antibiofilm Activity of Natural Products and Phytochemicals, *ACS Appl. Nano Mater.*, 2020, **3**, 8537–8556.

24 A. Ivask, *et al.*, Toxicity mechanisms in Escherichia coli vary for silver nanoparticles and differ from ionic silver, *ACS Nano*, 2014, **8**, 374–386.

25 A. Ivask, *et al.*, Size-Dependent Toxicity of Silver Nanoparticles to Bacteria, Yeast, Algae, Crustaceans and Mammalian Cells In Vitro, *PLoS One*, 2014, **9**, e102108.

26 S. A. Khan, M. Jain, K. K. Pant, Z. M. Ziora and M. A. T. Blaskovich, Photocatalytic Degradation of Methylparaben Using Green Nanosilver Supported on Reduced Graphene Oxide, *Ind. Eng. Chem. Res.*, 2023, **62**, 6646–6659.

27 A. Kyrychenko, D. A. Pasko and O. N. Kalugin, Poly(vinyl alcohol) as a water protecting agent for silver nanoparticles: the role of polymer size and structure, *Phys. Chem. Chem. Phys.*, 2017, **19**, 8742–8756.

28 G. Macindoe, L. Mavridis, V. Venkatraman, M. D. Devignes and D. W. Ritchie, HexServer: an FFT-based protein docking server powered by graphics processors, *Nucleic Acids Res.*, 2010, **38**, W445–W449.

29 H. Dang and C. R. Lovell, Microbial Surface Colonization and Biofilm Development in Marine Environments, *Microbiol. Mol. Biol. Rev.*, 2016, **80**, 91–138.

30 J. Ma, J. Zhang, Z. Xiong, Y. Yong and X. S. Zhao, Preparation, characterization and antibacterial properties of silver-modified graphene oxide, *J. Mater. Chem.*, 2011, **21**, 3350–3352.

31 W. P. Xu, *et al.*, Facile synthesis of silver@graphene oxide nanocomposites and their enhanced antibacterial properties, *J. Mater. Chem.*, 2011, **21**, 4593–4597.

32 S. Park, *et al.*, Biocompatible, Robust Free-Standing Paper Composed of a TWEEN/Graphene Composite, *Adv. Mater.*, 2010, **22**, 1736–1740.

33 J. M. R. Moreira, *et al.*, The effect of glucose concentration and shaking conditions on Escherichia coli biofilm formation in microtiter plates, *Chem. Eng. Sci.*, 2013, **94**, 192–199.

34 J. Jara, *et al.*, Self-Adaptation of Pseudomonas fluorescens Biofilms to Hydrodynamic Stress, *Front. Microbiol.*, 2021, **11**, 588884.

35 S. K. R. Namasivayam and E. A. Roy, Enhanced antibiofilm activity of chitosan stabilized chemogenic silver nanoparticles against Escherichia coli, *Int. J. Sci. Res. Publ.*, 2013, **3**(4).

36 P. Jena, S. Mohanty, R. Mallick, B. Jacob and A. Sonawane, Toxicity and antibacterial assessment of chitosancoated silver nanoparticles on human pathogens and macrophage cells, *Int. J. Nanomed.*, 2012, **7**, 1805–1818.

37 B. Malaikozhundan, *et al.*, Antibacterial and antibiofilm assessment of Momordica charantia fruit extract coated silver nanoparticle, *Biocatal. Agric. Biotechnol.*, 2016, **8**, 189–196.

38 K. Kalishwaralal, S. BarathManiKanth, S. R. K. Pandian, V. Deepak and S. Gurunathan, Silver nanoparticles impede the biofilm formation by Pseudomonas aeruginosa and Staphylococcus epidermidis, *Colloids Surf. B Biointerfaces*, 2010, **79**, 340–344.

39 M. A. Ansari, H. M. Khan, A. A. Khan, S. S. Cameotra and M. A. Alzohairy, Anti-biofilm efficacy of silver nanoparticles against MRSA and MRSE isolated from wounds in a tertiary care hospital, *Indian J. Med. Microbiol.*, 2015, **33**, 101–109.

40 D. Banerjee, *et al.*, A Review on Basic Biology of Bacterial Biofilm Infections and Their Treatments by Nanotechnology-Based Approaches, *Proc. Natl. Acad. Sci. India B Biol. Sci.*, 2019, **90**(2), 243–259.

41 S. L. Percival, P. G. Bowler and D. Russell, Bacterial resistance to silver in wound care, *J. Hosp. Infect.*, 2005, **60**, 1–7.

42 S. Mohanty, *et al.*, An investigation on the antibacterial, cytotoxic, and antibiofilm efficacy of starch-stabilized silver nanoparticles, *Nanomedicine*, 2012, **8**, 916–924.

43 C. K. Hope and M. Wilson, Analysis of the Effects of Chlorhexidine on Oral Biofilm Vitality and Structure Based on Viability Profiling and an Indicator of Membrane Integrity, *Antimicrob. Agents Chemother.*, 2004, **48**, 1461–1468.

44 L. G. Ferreira, R. N. Dos Santos, G. Oliva and A. D. Andricopulo, Molecular Docking and Structure-Based Drug Design Strategies, *Molecules*, 2015, **20**, 13384–13421.